Title

THE TEMPERATURE OF THE COSMIC MICROWAVE BACKGROUND RADIATION AT A FREQUENCY OF 10 GHz

Author

Kogut, A.

Publication Date

1987-05-01

LBL-23485
Preprint

Lawrence Berkeley Laboratory
UNIVERSITY OF CALIFORNIA

Physics Division

Submitted to Astrophysical Journal

THE TEMPERATURE OF THE COSMIC MICROWAVE BACKGROUND RADIATION AT A FREQUENCY OF 10 GHz

A. Kogut, M. Bersanelli, G. De Amici,
S.D. Friedman, M. Griffith, B. Grossan,
S. Levin, G.F. Smoot, and C. Witebsky

May 1987

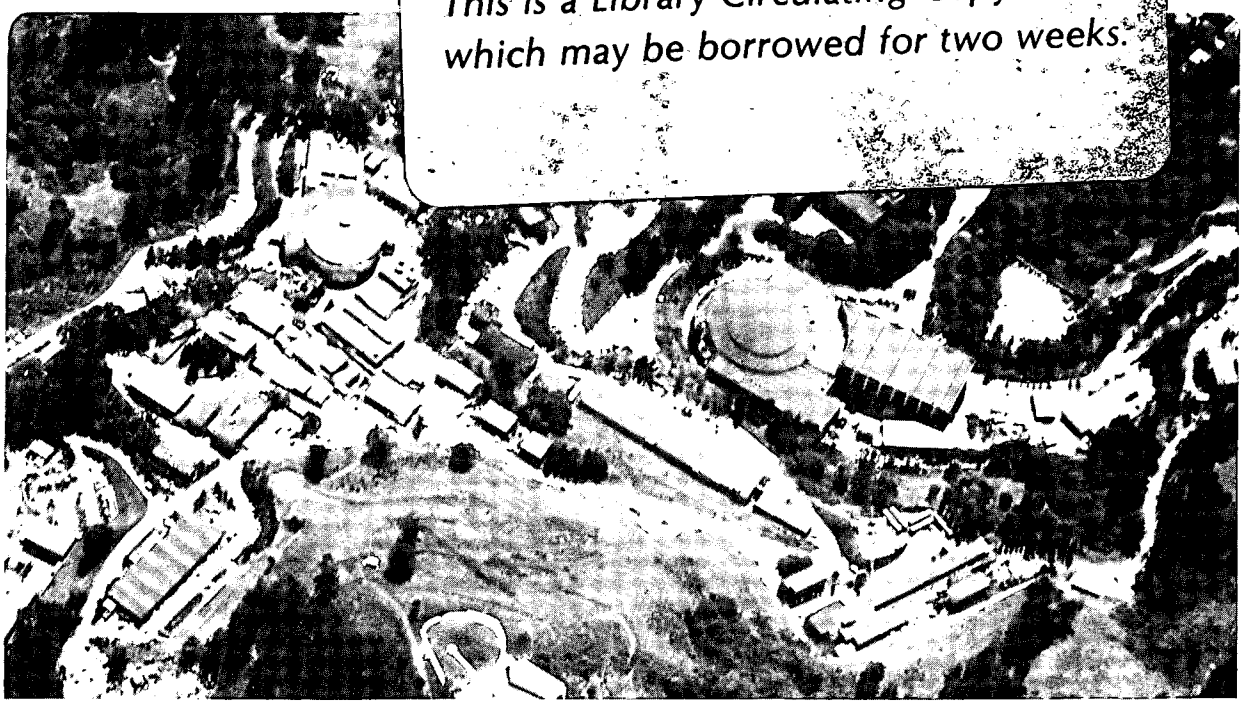

Prepared for the U.S. Department of Energy under Contract DE-AC03-76SF00098

DISCLAIMER

THE TEMPERATURE OF THE COSMIC MICROWAVE BACKGROUND RADIATION AT A FREQUENCY OF 10 GHZ

A. KOGUT, M. BERSANELLI, G. DE AMICI, S. D. FRIEDMAN,[1] M. GRIFFITH,[2]

B. GROSSAN,[2] S. LEVIN, G. F. SMOOT, AND C. WITEBSKY

Space Sciences Laboratory

and

Lawrence Berkeley Laboratory
University of California
Berkeley, CA 97420

[1]Now at the University of California, San Diego.

[2]Now at the Massachusetts Institute of Technology.

ABSTRACT

We have measured the temperature of the cosmic microwave background radiation (CMBR) at a frequency of 10 GHz (wavelength 3.0 cm) as part of a larger effort to determine the spectrum of the CMBR in the Rayleigh-Jeans region. The instrument used is a superheterodyne Dicke-switched radiometer. We have repeated the measurement over four summers with successively improved techniques and equipment. Our best estimate of the CMBR thermodynamic temperature at 10 GHz is 2.61 $\pm$ 0.06 K, where the error estimate is a 68% confidence level limit.

Subject headings: cosmic background radiation

I. INTRODUCTION

The spectrum of the cosmic microwave background radiation (CMBR) constrains energy-releasing processes in the early universe (Danese and De Zotti 1977). Energy injected into the CMBR (from turbulent processes, particle decay, or other mechanisms) distorts the spectrum from a Planckian distribution. If the energy transfer occurs at a redshift less than a few times 10^6, there is insufficient time for the radiation field to thermalize to a new Planckian distribution; a combination of Compton scattering and bremsstrahlung results in a distorted (non-thermal) CMBR spectrum (Sunyaev and Zel'dovich 1970; Danese and De Zotti 1980). The existing data allow large (200 mK) deviations in the long-wavelength Rayleigh-Jeans portion of the spectrum (Danese and De Zotti 1978).

To provide better measurements of the Rayleigh-Jeans portion of the spectrum, we entered an international collaboration in 1979, the results of which have been reported elsewhere (Smoot *et al.* 1983, 1985*a*). The 10 GHz radiometer described here was a part of that collaboration, and took data in 1982 and 1983. In 1984, the Berkeley group modified the 10 GHz radiometer to allow automated atmospheric measurements. In 1986, the radiometer was used once again, with further modifications to reduce systematic errors observed in previous years. This paper describes the 10 GHz radiometer and the results of measurements taken with it between 1982 and 1986.

II. EXPERIMENTAL CONCEPTS AND DESIGN

The output of a radiometer is proportional to the power P received by the antenna within a finite bandwidth B. The radiometer is calibrated in units of antenna temperature T_A, which is related to the thermodynamic temperature T of a blackbody completely filling the antenna aperture by the relation

$$T_A = \frac{P}{kB} = \frac{x}{(e^x - 1)} T \, ,$$

where $x = h\nu/kT$, ν is frequency, h is Planck's constant, and k is Boltzmann's constant.

The antenna temperature of the zenith sky, $T_{A,\mathrm{zenith}}$, is measured by comparing the output of

the radiometer viewing the zenith sky to the output viewing a load of known temperature, $T_{A,\mathrm{load}}$:

$$T_{A,\mathrm{zenith}} - T_{A,\mathrm{load}} = G(V_{\mathrm{zenith}} - V_{\mathrm{load}}) ,$$

where G is the calibration coefficient (inverse gain) of the radiometer and V_{zenith} and V_{load} are the output voltages of the radiometer viewing the zenith or load, respectively. The sky signal is the sum of signals from the CMBR, the atmosphere, the galaxy, and extraneous ground radiation entering through the antenna sidelobes, where we have neglected (for purposes of this discussion but not in the actual analysis) the small attenuation of the CMBR signal by the atmosphere:

$$T_{A,\mathrm{zenith}} = T_{A,\mathrm{CMBR}} + T_{A,\mathrm{atm}} + T_{A,\mathrm{galaxy}} + T_{A,\mathrm{ground}} . \quad (1)$$

The antenna temperature of the CMBR is the residual after the atmospheric, ground, and galactic signals have been subtracted from the measured zenith sky temperature:

$$T_{A,\mathrm{CMBR}} = G(V_{\mathrm{zenith}} - V_{\mathrm{load}} + T_{A,\mathrm{load}} - T_{A,\mathrm{atm}} - T_{A,\mathrm{ground}} - T_{A,\mathrm{galaxy}}) . \quad (2)$$

We have chosen a wavelength of 3.0 cm to minimize the two largest residual signals, atmospheric and galactic emission. Figure 1 shows galactic and atmospheric emission spectra for low frequencies at a high-altitude site. Galactic emission is highly anisotropic, with a maximum in the galactic plane. At low frequencies it is dominated by thermal (HII emission) and non-thermal (synchrotron) radiation, and rises steeply at lower frequencies. Atmospheric emission at 10 GHz is primarily from oxygen continuum; a small component is due to residual water vapor. On time scales of a few hours, only the component due to water vapor fluctuates; observing from a dry, high-altitude site reduces both the water vapor content and variability. Accordingly, we have performed all measurements from the Nello Pace Laboratory of the Barcroft Facility, White Mountain Research Station of the University of California, situated at an altitude of 3800 meters in the White Mountains of eastern California (latitude 38°). The site lies in the rain shadow of the Sierra Nevada range and has typical water vapor column density below 0.5 g cm^{-2}. Atmospheric signal magnitude and variability are reduced by a factor of three compared to measurements taken

near sea level in Berkeley, California.

To reduce systematic errors as much as possible, we measure the contribution of the atmosphere (which constitutes more than 99% of the last three terms in Equation 2) with the same instrument used to measure the zenith sky temperature. By proper design of the experiment, remaining systematic uncertainties in the result may be reduced to a low level.

We measure the first four quantities of Equation 2 (zenith sky, cold load, atmospheric, and ground signals) at nearly the same time and with the same instrument. Only the small galactic contribution is modeled, from measurements at lower frequencies appropriately scaled to 10 GHz. The galactic model agrees well with measurements at 10.4 GHz (Davies *et al.* 1987) and with upper limits at 10 GHz (this work).

The cryogenically cooled reference target, shown in Figure 2, has been described elsewhere (Smoot *et al.* 1983) and is shared with other radiometers. It consists of a microwave absorber in a large (0.7 m) open-mouth dewar covered by two windows of 23-micron polyethylene film. The absorber is submerged beneath ambient-pressure liquid helium (LHe) and acts as a microwave blackbody in an oversized multimode waveguide. The helium boiling temperature is calculated from the measured ambient barometric pressure and converted to antenna temperature. Emission from the polyethylene windows contributes 5 ± 2 mK; resistive losses in the walls contribute 9 ± 5 mK; the power emitted by the radiometer and reflected by the absorber contributes 7 ± 4 mK (Friedman 1984). The coherence length of the radiometer is small enough that coherent reflection is not a problem; coherent reflections from the target and the radiometer contribute 0 ± 10 mK to the total load signal. Summing these signals, the antenna temperature of the cold load is

$$\begin{aligned} T_{A,\mathrm{load}} &= 3.562 \pm 0.013 \text{ K } (1982 - 1984) \\ &= 3.568 \pm 0.013 \text{ K } (1986) . \end{aligned}$$

The higher value for 1986 is the result of a slightly higher ambient pressure in the cold load that year.

We measure the zenith sky temperature $T_{A,\mathrm{zenith}}$ by comparing the output of the radiometer as

it alternately views the cold load and the zenith sky. At 10 GHz on White Mountain, the zenith sky is within 100 mK of the cold load, which greatly reduces the dependence of the CMBR result on precise knowledge of the absolute calibration.

We measure the atmospheric temperature $T_{A,\mathrm{atm}}$ by correlating the signal change with the air mass in the beam as the radiometer beam scans different zenith angles. Using the same radiometer to measure both the atmospheric and zenith sky temperatures eliminates a large source of potential systematic uncertainty. We further reduce uncertainty in the atmospheric results by measuring the atmosphere in two independent ways and correlating the results with atmospheric measurements performed at the same time at other frequencies.

We calibrate the radiometer by comparing its output as it alternately views targets of known, dissimilar temperature. The use of targets at widely different temperatures (LHe and ambient) reduces the precision to which each temperature must be known. A third, intermediate-temperature target (liquid nitrogen, LN) allows the small saturation effects to be calculated. The calibration is monitored to better than 1% throughout the measurement.

The use of a Dicke-switched radiometer viewing similar-temperature targets in close succession reduces the effects of absolute calibration uncertainties and drifts to low levels. A calibration uncertainty of 1% corresponds to an uncertainty of 12 mK in the atmospheric temperature and less than 1 mK in the zenith sky temperature. Proper use of a Dicke-switched radiometer requires a stable, cold reference target. We use the zenith sky for a reference, either viewed directly (primary antenna) or reflected by an aluminum mirror (secondary antenna). The radiometer is designed to allow the two antenna beams to scan independently.

III. DESCRIPTION OF THE RADIOMETER

The radiometer used throughout the experiment is a superheterodyne Dicke-switched radiometer with a passband from 9.5 to 10.5 GHz, shown schematically in Figure 3. The two input ports are identical, conical, corrugated horn antennas, manufactured by CSELT of Torino, Italy, and designed to have low sidelobes. The measured half-power beamwidth is $12.^{\circ}5$, symmetric in

the E- and H-planes (Bielli *et al.* 1983).

The signal received by the antennas is fed through rectangular waveguides to an electromagnetic switch consisting of a latching ferrite three-port circulator. The switch has a measured insertion loss of less than 0.3 dB between any two coupled ports and has greater than 25 dB isolation between uncoupled ports. It is switched at 100 Hz by an external clock signal. The circulator allows the input horns to act as sky horns: when the switch connects one horn to the radiometer, power emitted by the radiometer is broadcast out the other horn, reducing reflection effects. An isolator located between the switch and the mixer further reduces the magnitude of the broadcast power. The measured isolation is greater than 36 dB.

The Gunn-effect local oscillator (LO) has output power of approximately 18 mW, which is reduced to approximately 10 mW by a waveguide attenuator. The LO is tuned to 10.00 $\pm$ 0.01 GHz as confirmed by a spectrum analyzer.

The mixer and intermediate-frequency (IF) pre-amplifier are a single unit with nominal bandpass 45–550 MHz and direct RF to IF gain of 24 dB. The difference frequency between the LO and sky signal, after preamplification, undergoes an additional 41 dB of amplification in a second IF amplifier with nominal bandpass 5-500 MHz. A 6 dB attenuator between the two amplifiers serves to decouple them and reduces non-linear saturation in the radiometer. The signal is rectified by a Schottky-barrier detector diode and fed to a lockin amplifier. The lockin consists of a demodulator synchronous with the switch and an ideal integrator which averages the demodulated signal for a 2-second period. The voltage gain of the lockin is approximately 1.5×10^4. The signal is then digitized and recorded on magnetic tape.

The sensitivity of a Dicke-switched radiometer is defined as the input temperature difference ΔT which gives rise to an output voltage equal to the RMS thermal noise fluctuations of the radiometer itself. For a system with square-wave switching and wide band detection this is given by (Kraus 1966)

$$\Delta T = 2\frac{T_{sys}}{(B\tau)^{1/2}}\,, \tag{3}$$

where T_{sys} is the system noise temperature, B is the IF bandwidth, and τ is the post-detection integration time. For this system, T_{sys}=490 K, B=455 MHz, which gives $\Delta T = 46$ mK for an integration time $\tau = 1$ second. The measured value is 46 $\pm$ 3 mK $Hz^{-1/2}$

All receiver components from Dicke switch onward are enclosed in RF-shielded, thermally-insulated boxes, as are the power supplies for the receiver and associated electronics. As the calibration coefficient of the radiometer is sensitive to changes in the temperature of the receiver components, thermal control circuits regulate the temperature of the plate and the power-supply box to within 0.1 K. We also monitor the temperatures of the Dicke switch, the power-supply box, both antennas, and the plate containing the mixer, IF amplifiers, and detector diode. The horns are too large and exposed to regulate; however, temperature drifts in the horns are slow compared to the period over which a single measurement of the CMBR is made (160 to 256 seconds).

The radiometer is mounted on bearings and is free to rotate about a horizontal axis coincident with the symmetry axis of the secondary horn. The primary horn, mounted at right angles, may rotate though 360°. Stops on the bearing mounts allow the primary to point at angles of $\pm$30°, $\pm$40°, $\pm$90° degrees from the zenith, directly at the zenith (0°), or directly downward (180°, the position of the cold load). A mirror mounted at 45° to the secondary horn axis redirects the secondary beam to the sky.

The finite conductivity of the aluminum mirror contributes a small linearly polarized component to the signal received by the secondary horn. The rotation of the radiometer with respect to the fixed mirror then induces an angle-dependent modulation of the reference signal. To reduce the magnitude of the modulation, a quarter-wave plate is installed in the throat of the secondary horn. The quarter-wave plate consists of a thin Teflon card, which creates a phase difference of 90° between the components of incident radiation polarized along and across the card. Mounted at 45° to the rectangular waveguide, it has the effect of transforming linearly polarized radiation aligned with the rectangular waveguide into left-circularly-polarized radiation, and vice versa. The secondary arm of the receiver is then sensitive to left-circularly-polarized radiation and is insensitive to the orientation of incident linearly polarized radiation. The quarter-wave plate

is not perfect, and a small residual modulation exists. The magnitude, though, is reduced from approximately 70 mK to less than 5 mK.

The ambient calibration target consists of a slab of microwave absorber (Eccosorb CV-3) mounted in a thermally insulated box. Held over the primary horn, it completely fills the horn aperture. A temperature sensor buried within the absorber monitors the temperature to an accuracy of 0.1 K. The box is closed on all sides when not actually calibrating the radiometer to allow the entire absorber to maintain thermal equilibrium.

a) 1982 Configuration

The radiometer was first assembled in 1982. The primary horn could point to zenith angles of ±30° while the secondary viewed the sky reflected in a large rectangular aluminum mirror. The secondary horn faced due north; the primary horn swung in an east/west plane with negative zenith angles west. Ground screens constructed of wire mesh prevented extraneous ground radiation from entering the beam. One set of screens surrounded the secondary horn and mirror on the sides and bottom; another set surrounded the sides of the primary horn as it viewed the sky (Figure 4).

We took data by rotating the primary horn so that it alternately viewed the cryogenic target buried in the ground, the zenith sky, the atmosphere at zenith angles of -30° and +30°, and finally an ambient calibration target mounted at +90°. The radiometer viewed each target in turn for 32 seconds, then rotated to the next. Less than 4 seconds of each 32 were spent rotating the radiometer; the rest were devoted to collecting and averaging the signal.

b) 1983 Configuration

The small differential air mass between zenith angles of 30° and 0° magnified the effect of systematic errors on the calculated atmospheric temperature. In 1983, we added additional zenith angles of ± 40° to the allowed primary horn positions. This brought the tilted primary beam closer to the horizon; to provide adequate protection against diffracted ground radiation, the mesh screens about the primary horn were enlarged. The screens surrounding the secondary horn and

mirror were also enlarged, and mechanical support for the radiometer's electronics was improved. In all other respects, the radiometer in 1983 closely resembled the 1982 configuration.

c) 1984 Configuration

Atmospheric measurements taken with the primary horn were subject to a fairly large statistical scatter, due mostly to the small zenith angles used. In 1984, the rectangular mirror redirecting the secondary beam was replaced by a smaller elliptical mirror. This mirror rotated about an axis coincident with the secondary horn axis and could be stopped automatically to view any desired zenith angle to within 4′.

Two independent methods existed to measure the atmospheric temperature. Measurements with the primary antenna ("primary atmospheres") were made as part of the CMBR measurements. In addition, measurements with the secondary antenna ("secondary atmospheres") were made at other times throughout the night to provide a check on the primary results and to monitor the atmosphere while other radiometers performed CMBR measurements over the cold load. The secondary measurements took place on a platform located approximately 20 m from the cold load, rotated 25° to the west to take advantage of the horizon profile at the platform site. Positive zenith angles during secondary scans have an azimuth of 245°, negative zenith angles 65°. Primary atmospheric scans were changed to view the zenith twice per scan; primary scans now comprised the angles 180° (cold target), 0°, -40°, -30°, 0°, +30°, +40°, and +90° (ambient target), in sequence. The secondary scanned angles of +54°, +47°, +40°, +30°, 0°, -30°, -40°, -47°, and -54° in order, while the primary horn viewed the zenith sky as a convenient reference. Periodically, the scan was stopped and the radiometer calibrated with the ambient target held over the secondary horn.

The elliptical mirror was measured to intercept 99.7% of the secondary beam. To prevent signal modulation arising from the remaining 0.3%, a large mesh screen was erected behind the mirror to redirect to the sky any spillover that might otherwise view the ground. The mesh screens to the sides of the mirror were redesigned to allow the mirror to rotate, and enlarged again to prevent diffracted ground radiation from entering the redirected beam at the largest zenith

angles. Due to problems with the ground shields, the secondary atmospheric scans did not provide any useful data in 1984.

d) 1986 Configuration

Measurements made after 1984 showed that a combination of dust and dirt collecting on the wire mesh ground screens and ground radiation transmitted through the screens could add a signal of up to 10 K if the antenna directly viewed the screens. While part of this was due to the aging and oxidation of the wire mesh, prudence dictated that we build alternate ground shields. By 1986, the mesh screens had been replaced by aluminum sheet ground shields, with the exception of a small screen used around the primary during secondary atmospheric scans. Additional ground shields were added; the secondary horn/mirror were now completely shielded in all directions except up. To block diffracted ground radiation during secondary atmospheric scans, a set of extensions to the side shields was added. The extensions were fixed at a larger zenith angle than the side shields and undercut them; they were designed to substitute sky radiation for diffracted ground radiation. A set of quarter-wave traps on the original side shields further reduced the amount of diffracted radiation entering the secondary beam.

Data from 1984 showed that the quarter-wave plate in the throat of the secondary horn could move far from its optimal position, greatly reducing its effectiveness. Thermal stress from diurnal heating also bent the Teflon card, again reducing its effectiveness. In 1986, a shallow groove was cut to hold the card, and the card was removed during the day. New cards made for the 1986 measurements showed an improvement over past years; their performance did not deteriorate throughout the night.

Tests in 1986 showed a 100 mK signal modulation caused by a slight (10 arcmin) misalignment of the secondary horn's symmetry and rotation axes. Rotating the primary horn caused the beam spillover past the elliptical mirror to vary slightly with position. An oversized trapezoidal mirror was fitted over the elliptical mirror during primary CMBR scans. This removed the modulation.

With new confidence in the results of the secondary atmospheric scans, we altered the

data collection routine. Each night, secondary atmospheric measurements were made from the platform for about an hour, with all ground shields in place and a small mesh screen protecting the (reference) primary from the movement of nearby personnel. The mirror changed positions automatically every 32 seconds. We then carried the radiometer to the cold load, where the trapezoidal mirror was placed over the elliptical mirror and an aluminum ground shield placed around the primary. The side diffraction shields were not not needed for primary scans, where the secondary contribution needed only to be stable. After the usual CMBR measurements over the cold load, the radiometer was carried back to the platform, where it resumed secondary atmospheric scans until dawn. Repeated movement of the radiometer did not affect its performance. Figure 5 shows the radiometer in its 1986 configuration.

IV. SYSTEM PERFORMANCE TESTS

We made numerous tests of the radiometer and associated apparatus before and after each trip to White Mountain to assess the magnitude of effects contributing to the error budget. These tests were performed in Berkeley during nights when the atmosphere was stable enough to yield consistent results. We repeated the most critical tests at White Mountain to verify that no changes had occurred during the trip to the site.

a) Systematic Offset Change

The CMBR measurements and atmospheric measurements made with the primary horn compare data taken with the radiometer rotated to view various targets. As the radiometer rotates on its bearings, gravitational stresses on the components change. It is vital that these changing stresses do not systematically change the performance of the radiometer, either in offset or gain, where the offset is defined as the output signal for zero temperature difference between the two input ports. We have tested extensively to limit this effect.

In the simplest test, we covered the primary horn with an ambient-temperature Eccosorb target, completely filling the aperture. The secondary viewed the reflected sky. We then looked

for output changes as the radiometer rotated. This procedure tested all radiometer components except the primary horn upstream of the Dicke switch, and was quite sensitive to gain changes. To test the primary upstream of the switch, the primary must view a cold target. This may be either an Eccosorb target saturated in LN, or the sky viewed directly or through reflectors. In the latter two cases, the radiometer cart direction was reversed (or the reflectors interchanged) and the test repeated to separate instrumental asymmetries from signal asymmetries. In all cases, the radiometer was repeatedly moved between two or more positions for periods of approximately 17 minutes; the output was recorded every 32 seconds and digitally signal-averaged to improve the statistics.

Small signal variations were observed as the radiometer primary horn rotated, but they were not consistent in sign or value from test to test. Upper limits to signal variation induced by changing radiometer position are given in Table 1 for both warm and cold targets. The lack of consistency from test to test precluded the simple interpretation of warm and cold signals in terms of a combination of gain variation and offset change for both targets. Instead, we preferred a more conservative approach and took the magnitude of the cold target result as an upper limit on offset changes and the warm target result as an upper limit on gain variation. As we have taken the largest signal change observed in many tests rather than the average, the result is likely to be an overestimate of the actual systematic offset change during CMBR measurements.

In all years, the gain was seen to vary negligibly as a function of radiometer position. Maximum fractional gain variation measured with Eccosorb over the primary horn was less than 10^{-3}. Note that, for the 180° (straight down) position, it was impossible to use the sky as a cold target. In this case, a piece of LN-soaked Eccosorb was held over the primary horn and the output compared for the up and down positions. Prior to 1986, this placed an upper limit of 55 mK on the size of any output changes caused by radiometer rotation. The limiting factor was observed drifts in output commencing approximately 15 seconds after the LN-saturated target was placed over the horn. We assumed that this represented thermal drift in the target. Tests in 1986 with a new target revealed that the drifts were caused by the rapid cooling of the primary horn induced

by contact with LN. Tests performed with the horn temperature carefully controlled then gave a signal change of 6 ± 17 mK due to horn rotation, consistent with zero change and with the results obtained with ambient Eccosorb over the primary. Rapid horn cooling at White Mountain was not a problem, as the measured horn temperature changed by less than 1 K over a 40 minute observation.

b) Calibration Stability

Use of a Dicke-switched radiometer reduces effects of calibration variation, but does not eliminate them completely. An error of 1% in the calibration of the radiometer causes a 12 mK error in the atmospheric temperature, and thus in the CMBR temperature. We measured the calibration coefficient every 256 seconds during CMBR measurements, and approximately once every 15 minutes during secondary atmospheric scans. We therefore required the system calibration to be stable to 1% or better for at least this long.

We measured calibration stability by placing an ambient Eccosorb target over one horn while the other viewed the sky. Drifts as small as $\delta G/G = 10^{-3}$ produced output changes larger than radiometer or atmospheric noise and were easily observable. Maximum drift observed in all years was less than 3×10^{-3} in 17 minutes, easily satisfying our requirement.

c) Calibration Linearity

We calibrated the radiometer by comparing the output as the radiometer viewed targets of known, widely separated temperature. Saturation of the detector diode due to the large power emitted by the ambient target caused a slight decrease in signal from strict linearity. For the calibration to be accurate to 1%, this effect must be measured and included in the data analysis. Detector non-linearity was found two ways: by direct measurements of the detector diode, and by substitution of an intermediate-temperature (LN) target for the warm target. The second method had the advantage of testing the response of the entire detection chain, and provided the more accurate result. In this method, we alternately calibrated between the ambient target/zenith sky and a LN target/zenith sky. LN provided a convenient target in the linear regime of the detector.

We then measured the atmospheric signal, assumed a zenith sky temperature, calculated the system gain, and repeated until we achieved a self-consistent result. The ratio of system gain viewing LN and system gain viewing an ambient target provided the non-linear response of the system. The resulting detector saturation is shown in Table 2. The higher saturation value in 1982 was due to a faulty zener diode in the lockin amplifier, replaced after 1982; all other results were within experimental limits. Maximum calibration uncertainty was 1% in 1982 and 1983, and was negligible for 1984 and 1986.

d) Integration

The sensitivity of the radiometer, as defined in Equation 3, is inversely proportional to the square root of the observing time so long as the radiometer noise contains no time-dependent structure. As a basic test of radiometer performance, and as a planning tool to enable us to determine how best to use our limited observing time, we measured the period at which the white-noise assumption broke down. In this test, both horns viewed the same cold target (to prevent target variations from entering the analysis) while the data were averaged for longer and longer periods. Typically the zenith sky was used as a target. The RMS fluctuations in the data decreased as expected for periods up to 64 seconds, after which non-random radiometer fluctuations dominated. This corresponded to an RMS noise level of 5 mK, negligible for our purposes.

e) Magnetic Sensitivity

The Earth has a magnetic field of approximately 0.5 Gauss. The ferrite switch and isolator are the components most sensitive to changes in the external magnetic field; as the radiometer rotates, the changing relative orientation between radiometer components and external field could conceivably induce a position-dependent signal modulation. We minimized the effect by wrapping the switch and isolator in several layers of mu-metal foil. To ensure that enough foil is used to reduce the residual field to negligible levels, we erected large (1.5 m diameter) coils around the radiometer and tested for magnetic response at field strengths of 10 and 5 Gauss, oriented

perpendicular to the rotation axis of the radiometer. The largest response (1.5 mK/Gauss) contributed negligibly to the radiometer response, and was consistent with the limits established by the offset tests.

f) Polarization Response

A quarter-wave plate in the throat of the secondary horn transformed the small linear polarization of the signal emitted and reflected by the mirror into circular polarization. The transformation is not perfect, and a residual linearly polarized signal causes a position-dependent output modulation. We evaluated the effectiveness of the quarter-wave plate by recording the response of the radiometer to a known large polarized signal as the angle between the polarization vector and the radiometer was changed. The small polarized signal from the mirror has been measured and agreed with the expected signal within the limits of measurement. The resultant residual signal after installation of the quarter-wave plate had a maximum amplitude of 5 mK. This was consistent with the limits set by the offset tests, which included but did not separate polarization effects. The effectiveness of the quarter-wave plate depended slightly on its position within the secondary horn's throat. We measured the response of the plate each time it was installed.

g) Pointing

We determined the atmospheric temperature by correlating the total signal received at a given zenith angle with the air mass at that angle, using an atmospheric model. Both the accuracy and repeatability of the angles used have been tested many times. Prior to 1986, the primary horn was the major source of atmospheric information. The pointing was found to be accurate and repeatable to within 4′. In 1986, the secondary and rotating mirror provided the most accurate atmospheric information, while the primary provided the zenith sky measurement central to the CMBR determination. Each time the large trapezoidal mirror was placed over and then removed from the smaller rotating elliptical mirror, the previous absolute pointing of the rotating mirror was destroyed. Rather than spend the hours necessary to set the angles back to their precise

nominal positions, the angles were reset to within 30′ of the nominal positions and the actual positions recorded. Tests then showed the actual positions chosen were repeatable to 4′ or better. We accorded similar treatment to the primary horn in the interests of saving time, using the the recorded true pointing angles in the atmospheric analysis.

h) Sidelobe Reception

Extraneous ground radiation entering the beam sidelobes or diffracting over the shields into the inner beam represented a potentially large source of error in the measurement of the atmosphere and zenith sky. We preferred to measure the effect directly rather than rely on models based on beam patterns and shield/horizon profiles. We measured sidelobe reception over the shields by alternately raising and lowering large aluminum sheets as simple extensions to the existing ground shields. We recorded the output and looked for signal changes correlated with extension position. If any signal was observed, we repeated the test with successively larger shields until no further change was seen. The total signal change from the largest extension to no extensions was taken as the magnitude of the sidelobe signal. A similar procedure tested for radiation diffracting over the shields, with the single exception that the additional shields were not held at the same angle as the main shield, but at a shallower angle. We tested the primary horn at all angles in all years. No sidelobe signal was ever observed at zenith. Small (typically 3 mK) signals were seen at 40°; these were consistent in any given year and were subtracted from the data at the appropriate angles. The secondary has also been tested since its inception in 1984. Sidelobe reception of up to 20 mK was observed in 1984; improved ground shields in 1986 reduced this to below 3 mK at all angles.

i) Primary Screen Interference

During secondary atmospheric measurements, we placed a small mesh screen around the primary horn to prevent the movement of nearby personnel from affecting the reference beam. Tests after we returned to Berkeley in 1986 showed that this screen itself caused a signal modulation dependent upon the mirror position. We measured the effect in Berkeley in two ways.

We alternately removed and replaced the screen and checked for effects correlated with screen position. We also performed alternate atmospheric scans with and without the screen. The two methods gave results in agreement with each other; the effect ranged from 70 mK at -30° to 140 mK at +47°. We removed this effect from the 1986 secondary data.

V. DATA REDUCTION AND ANALYSIS

To measure the antenna temperature of the CMBR, $T_{A,\mathrm{CMBR}}$, we independently measured the zenith sky temperature $T_{A,\mathrm{zenith}}$ and the atmospheric temperature $T_{A,\mathrm{atm}}$. We then obtained $T_{A,\mathrm{CMBR}}$ by solving Equation 2.

The voltage output of the radiometer was digitized with a 16-bit analog-to-digital converter (ADC) and recorded in digitized units (du). Housekeeping information (temperatures within the radiometer, beam pointing, ambient temperature and pressure) was also recorded. Data taken between positions were discarded, and the rest used for analysis. Analysis proceeded on a scan-by-scan basis. First, the calibration was calculated (for scans with a LN or LHe cold load) or estimated (for secondary atmospheric scans which use the zenith sky as a second calibration load). Corrections to the data were made, the galactic contribution removed, and the sky and atmospheric temperatures calculated. For secondary atmospheric scans the calibration, zenith sky and atmospheric temperatures were recalculated to obtain a self-consistent result.

a) Calibration

We measured the calibration coefficient G of the system using an ambient target and a cold load:

$$G = \frac{1}{S}\,\frac{T_{A,\mathrm{amb}} - T_{A,\mathrm{load}}}{V_{\mathrm{amb}} - V_{\mathrm{load}}}\,,$$

where S is the gain saturation factor (Table 2); $T_{A,\mathrm{amb}}$ is the antenna temperature of the ambient target; $T_{A,\mathrm{load}}$ is the antenna temperature of the LHe load; V_{amb} is the radiometer output viewing the ambient target; and V_{load} is the radiometer output viewing the LHe load. The value of G was roughly 9 mK/du in all years, adjusted so the largest signal difference (ambient–sky, approximately 300 K) remained on the ±32767-du scale of the ADC.

b) Atmospheric Antenna Temperature

If the antenna beam were a delta function, the atmosphere were a flat slab, and no sources existed external to the atmosphere, the atmospheric antenna temperature would be given by

$$T_{A,\mathrm{atm}} = G\frac{V_\theta - V_{\mathrm{zenith}}}{\sec(\theta) - 1}\ , \tag{4}$$

where V_{zenith} is the radiometer output viewing the zenith sky, and V_θ is the radiometer output at zenith angle θ.

In practice, the antenna beam has a 12°.5 half-power beamwidth, the atmosphere follows the curve of the Earth, external radiation is attenuated differently at different angles, and highly anisotropic sources of radiation exist external to the atmosphere (*e.g.* the galaxy). These effects are small (the optical depth of the atmosphere $\tau \approx 0.005$; a curved atmosphere deviates from a flat one by 0.2% at 40°) and partly cancel; the total difference between Equation 4 and the atmospheric model used amounts to about 50 mK. The model used is similar to that used by Witebsky *et al.* (1986), with a single ambient atmospheric temperature of 240 K and a single scale height of 7 km for O_2 and H_2O. Uncertainty in these parameters contributes negligibly to the atmospheric uncertainty; the dominant uncertainty in the model is the convolution of the beam pattern with the atmosphere.

The galactic signal, although less than 30 mK at 10 GHz, does have the potential to affect the atmospheric calculations. In summer at White Mountain, the atmospheric scans can cut through the galactic plane. The differential galactic signal between zenith and the angle θ is multiplied by approximately $[\sec(\theta) - 1]^{-1}$ in the atmospheric calculations. At 40°, this triples the effect of the signal. We subtracted the galactic signal from the data using galactic maps compiled from data at lower frequencies (Haslam *et al.* 1982) and extrapolated to 10 GHz. An error in the extrapolated values as great as 50% would, in the worst case, affect the measurement at one atmospheric angle by less than 40 mK, or the mean $T_{A,\mathrm{atm}}$ by less than 10 mK.

The automated atmospheric scans taken in 1986 provided a direct upper limit to the magnitude of the differential galactic signal. Data in which the galactic plane has moved through

the beam at one angle were indistinguishable from reference data at other angles far from the plane. This placed an upper limit of 30 mK on the peak magnitude of the galactic signal, limited by atmospheric drifts over several hour intervals, and consistent with model predictions of 25 mK peak differential signals.

After corrections for galactic and minor sidelobe contributions, the data at various angles were averaged to get one value for the atmospheric temperature for each scan. In 1982 through 1984, we took $T_{A,\mathrm{atm}}$ at each angle θ to be the mean of the values at $\pm\theta$. This procedure reduced the effects of an overall tilt in the radiometer cart to less than 10 mK, so long as the *relative* separation of the angles was correct to 10′. The mean value was assigned an uncertainty; we then took a weighted average of the 30° and 40° results. The statistical and (weighted) systematic uncertainties were added in quadrature; the resulting uncertainty was dominated by systematic effects, primarily limits to the systematic offset change.

In 1986, the most accurate atmospheric data came from the secondary measurements, which were not subject to an offset change. Eight independent measurements were made each scan. We made an additional correction for the effects of the primary screen modulating the secondary signal. After correction, the data still showed a systematic spread of about 130 mK, with +54° consistently highest and -30° lowest. The effect may be due to uncertainty between the screen modulation effect at White Mountain and as measured in Berkeley with a different horizon profile. As the spread was larger than the individual systematic errors discussed above, we did not weight each angle but instead simply took the mean of all 8 values. We took half the value of the total spread in the data as a conservative estimate of the systematic uncertainty and added it in quadrature with the small statistical uncertainty. The resultant uncertainty was still smaller than the uncertainty in the primary atmospheric measurements; the atmospheric temperatures obtained by both methods were in excellent agreement. Table 3 shows the measured atmospheric temperature for 1982–1986.

The secondary atmospheric data were not taken simultaneously with the zenith sky measurement. 90 GHz (0.33 cm) atmospheric scans showed a smooth linear drift of atmospheric

temperature throughout the night. Accordingly, we obtained the 10 GHz atmospheric temperature by linear interpolation of the secondary atmospheric data. The resulting 10 GHz atmospheric temperatures for the times of the zenith sky measurement are shown in Table 4, along with the results of (noisier) primary atmospheric scans taken during zenith sky measurements.

Comparison of atmospheric results from all four years is a useful check against possible systematic effects. Figure 6a shows the 10 GHz atmospheric antenna temperature plotted against the atmospheric antenna temperature measured simultaneously at 90 GHz, an independent measure of the atmosphere. The 1982 values are all anomalously low, indicative of either anomalous atmospheric behaviour or a systematic error. In addition, the 1982 atmospheric data did not support the result of measurements taken by our collaborators at nearby frequencies (Partridge *et al.* 1984). We have additional atmospheric information in the form of the zenith sky temperature, which is roughly the sum of a constant CMBR term and a variable atmospheric term (Equation 1). Figure 6b shows the measured sky temperature at 10 GHz, also plotted against the 90 GHz atmospheric temperature. The data correlate well; in particular, the 1982 result shows no sign of atmospheric anomalies at either 10 or 90 GHz. Any true atmospheric effect should appear in both plots; as it does not, we conclude that the previously reported 1982 atmospheric temperatures are too low by approximately 0.23 K. This is easily understood if a systematic offset of 0.03 K were present; at zenith angles of 30° used in 1982, the effect of any offset change on the atmospheric calculations is multiplied by more than six. The previously quoted uncertainty of 0.16 K for the 1982 atmospheric temperature is probably an underestimate, as this value used the average of many offset tests rather than the maximum reported in Table 1.

A better estimate of the 1982 atmospheric temperature may be obtained by using the correlation between the atmospheric temperature at 10 and 90 GHz as measured from 1983 to 1986, for which the data show no evidence of systematic effects. The best-fit line to the 1983-86 atmospheric data has a slope 0.013 ± 0.005 and an intercept 1.012 ± 0.075 K, compared to a theoretical slope of 0.019 ± 0.001 and an intercept of 0.88 ± 0.08 K (Costales *et al.* 1986). From this and the measured 1982 atmospheric temperature at 90 GHz, we obtain the estimated 10 GHz

atmospheric temperature shown in Table 5. As the atmosphere at 10 GHz may change by more than 50 mK over several hours, we do not attempted to calculate temperatures for those times during which 90 GHz data are not available.

The resultant atmospheric and sky measurements form a self-consistent data set. Figure 7 shows the measured zenith sky temperature plotted against the corrected atmospheric temperature for 1982-1986. The zenith sky temperature measurements include an atmospheric component, but are much less sensitive to systematic effects than the atmospheric measurements. Ignoring a small (<15 mK) galactic component, the data should correlate with a unity slope and an intercept equal to the CMBR antenna temperature. The data are in statistical agreement with the expected fit, indicating there are no serious undetected systematic errors.

VI. RESULTS

As is usually the case in CMBR measurements, our uncertainty in the CMBR temperature is dominated by systematic effects. The atmosphere is the largest background signal in the experiment; in every year, the total systematic uncertainty is dominated by the uncertainty in the atmospheric temperature. We have used three different methods to calculate the atmospheric temperature, with correspondingly different systematic effects. As stated above, we derive an atmospheric temperature for 1982 by correlating results at 90 GHz with results at 10 GHz taken in later years. The atmospheric uncertainties of 1983 and 1984 are dominated by upper limits to possible systematic angle-dependent changes in offset. Secondary atmospheric measurements are not subject to this effect; the 1986 atmospheric uncertainty is dominated instead by the interference of the primary screen, an effect not present during primary atmospheric measurements.

Table 6 shows all contributions to the atmospheric systematic uncertainty for a typical year, 1983. The source terms may vary independently; the total uncertainty at each atmospheric angle is thus the quadrature sum of the individual atmospheric terms. The data at each angle are independent of data at other angles. We weight the atmospheric data at each angle by the

corresponding uncertainty; the uncertainty in the result is given by the inverse squared sum of the individual uncertainties, as shown in the bottom row of Table 6. Values for 1984 or 1986 may be found by using the appropriate values for offset and gain variation from Tables 1 and 2.

Table 7 shows all systematic effects for the CMBR measurement (zenith sky minus atmospheric and other signals, Equation 2). After the atmospheric contribution, the major components are from the cold load and systematic offset changes. While uncertainties in the absolute load signal do not correlate with atmospheric uncertainties, systematic offset changes due to changing radiometer position may, and must be considered. Although tests reveal small differences in radiometer performance as the zenith angle varies, the differences each year are not consistent from test to test. We take the largest differences each year as upper limits to the magnitude of any angle-dependent effect (Table 1). The effect at any angle is not correlated with the effect at any other angle; in particular, the up-down offset change is not observed to correlate with the zenith-θ atmospheric offset change. Accordingly, we add the limits on offset change in quadrature with the atmospheric and other systematic effects to derive a total systematic uncertainty on the CMBR temperature.

We find the CMBR antenna temperature $T_{A,\mathrm{CMBR}}$ by evaluating the terms in Equation 2, shown in Table 8 as averages over each run. The most important terms are the zenith sky – cold load temperature difference $G\Delta V$ (column 4) and the atmospheric antenna temperature $T_{A,\mathrm{atm}}$ (column 6). These data are consistent and correlate as expected. To obtain the best estimate of the CMBR temperature, we solve Equation 2 on a scan-by-scan basis for each year and fit the resultant CMBR data to a Gaussian. The resultant CMBR temperatures for all four years are shown in Table 9. The statistical scatter of the CMBR data after the atmosphere and other signals have been removed is given in column 4; the total uncertainty is the quadrature sum of the statistical uncertainty and the systematic uncertainties of Table 7.

The CMBR data from 1982 to 1984 were well described by Gaussian distributions. In 1986, we obtained only 26 data points, which showed a much larger RMS than expected. Each data point was the average of one scan, and had an associated uncertainty consistent with that expected

from radiometer noise. From one scan to the next, however, there were large (~100 mK) jumps which could not be explained by radiometer noise alone. We conjecture that the jumps were caused by equipment shocks induced by rapid movement of the radiometer between positions while taking data at White Mountain, causing a random shift in the offset. Shocks would be expected to generate random offset changes of either sign, independent of angle, whose average over many repetitions is zero. This is supported by the observed behaviour of the effect: the output changed relative to the previous scan only at the 180° and 0° positions, for which the largest movement and shocks were generated. No effect was observed in offset tests, which involved much gentler movements of the instrument and test for repeatable non-random systematic changes. Integration tests with both horns viewing the zenith taken between two runs over the cold load showed no effect, ruling out most intermittent sources of interference whose signal would not be expected to average to zero (ground loops, interference with other radiometers, radio-frequency interference). We concluded that the effect served to inject noise to the output signal at 0°and 180°, but did not alter the mean of the signal difference between the two angles when averaged over many scans. With this additional source of noise, the RMS noise of the data integrated down to the 47 mK level. We took the value of 47 mK as a 68% confidence level for the estimate of the uncertainty of the mean of the parent distribution.

The final 1986 uncertainty of 83 mK was still dominated by the systematic uncertainty in the atmospheric measurement. In the unlikely event that the effect causing the increased RMS also changed the mean, the most conservative estimate of the uncertainty is 180 mK, half the total spread in the 1986 data. As the 1986 results were in agreement with the results of previous years, there is no statistically significant evidence to justify such a procedure.

Column 5 of Table 9 lists the thermodynamic temperature of the CMBR as determined each year, along with the total estimated uncertainty. The uncertainty is dominated in each year by different systematic effects. The 90 GHz correlation uncertainty, any angle-dependent offset changes, and the primary screen interference are all independent effects. The results for all years are in agreement with each other. Since most of the total uncertainty is systematic, not statistical,

and since the systematic uncertainty is largely independent each year, we have averaged the values in Table 9 weighted by their total estimated uncertainty. The resultant CMBR thermodynamic temperature at 10 GHz is

$$T_{A,\mathrm{CMBR}} = 2.61 \pm 0.06 \text{ K}.$$

The combined result differs from previously published estimates of the CMBR temperature using the same radiometer (Smoot *et al.* 1985*a*,*b*) by more than the estimated error. This is largely due to reanalysis of the 1982 atmospheric temperature made possible by three years of additional atmospheric data at 10 and 90 GHz. The smaller uncertainty is largely due to the use of the secondary atmospheric scans in 1986, which have greatly improved our ability to monitor the temperature of the atmosphere.

VII. COMPARISON WITH RELATED MEASUREMENTS

Prior to the start of our effort, the only CMBR measurements near 3.0 cm wavelength were taken at 3.2 cm shortly after the discovery of the existence of the CMBR. Roll and Wilkinson (1966) reported $T_{A,\mathrm{CMBR}} = 3.0 \pm 0.5$ K, while Stokes *et al.* (1967) reported a CMBR temperature of $2.69^{+0.16}_{-0.21}$. These data are in agreement with our results. Table 10 lists results of recent CMBR spectral measurements across a wider frequency range. Taken together, these data are consistent with an undistorted blackbody with a temperature of 2.741 ± 0.016 K. The strictest limits on energy-releasing processes in the early universe occur for energy released at a redshift z between 10^5 and 10^6. Compton-scattering distorts the CMBR spectrum to higher frequencies, while bremsstrahlung has largely filled in the low-frequency deficit with new photons, leaving a narrow colder transition region in the low-frequency spectrum (Danese and De Zotti 1980). The best fit to such a spectrum yields a fractional energy release $\Delta E/E_{CMBR} = 0.0015$ with χ^2 of 21.2 for 16 degrees of freedom. Fits to an undistorted spectrum ($\Delta E/E$=0) by comparison have $\chi^2 =$ 22.5 for 17 DOF. (The cosmological baryon density parameter Ω_b has been taken to be 0.1 for the purposes of this discussion). A more complete discussion of the CMBR spectrum and resulting cosmological implications will be published in a forthcoming paper (Smoot *et al.* 1987*b*).

ACKNOWLEDGEMENTS

We gratefully acknowledge the skilled help of many people over the course of this experiment: J. Aymon, H. Dougherty, J. Gibson, N. Gusack, F. Mitschang, and the staff and crew of the White Mountain Research Station. This work was supported by NSF grants PHY 80-15694 and AST 800737, by the Department of Energy under Contract DE-AC03-76SF00098, by C.N.R. Fellowships nos. 203.2.13 and 203.2.15, and by ISTRA (Milano).

REFERENCES

Bielli, P., Pagana, E., and Sironi, G. 1983, *Proceedings ICAP,* **1**, 509.

Davies, R. D., Lasenby, A. N., Watson, R. A., Daintree, E. J., Hopkins, J., Beckman, J., Sanchez-Almeida, J., and Rebolo, R. 1987, *Nature,* **326**, 462.

Costales, J. B., Smoot, G. F., Witebsky, C, De Amici, G., and Friedman, S. D. 1986, *Radio Science,* **21**, 47.

Crane, P., Heygi, D. J., Mandolesi, N., and Danks, A. C. 1986, *Ap. J.,* **309**, 822.

Danese, L., and De Zotti, G. 1977, *Riv. Nuovo Cimento,* **7**, 277.

——. 1978, *Astr. Ap.,* **68**, 157.

——. 1980, *Astr. Ap.,* **84**, 364.

De Amici, G., Smoot, G. F., Aymon, A., Bersanelli, M., Kogut, A., Levin, S. M., and Witebsky, C. 1987, submitted to *Ap. J.*

Friedman, S. D. 1984, Ph.D. Thesis, Univ. of Ca. Berkeley, LBL #17279.

Haslam, C. G. T., Salter, C. J., Stoffel, H., and Wilson, W. E. 1982 *Astr. Astroph. Suppl. Ser.,* **47**, 1.

Johnson, D. G., and Wilkinson, D. T. 1986, *Ap. J. Lett,* **320**, L1-L3.

Kraus, J.D. 1966, *Radio Astronomy* (New York: McGraw-Hill).

Mandolesi, N., Calzolari, P., Cortiglioni, S., Morigi, G. 1986, *Ap. J.,* **310**, 561.

Meyer, D. M., and Jura, M. 1985, *Ap. J.,* **297**, 119.

Partridge, R. B., Cannon, J., Foster, R., Johnson, C., Rubinstein, E., Rudolph, A., Danese, L., and De Zotti, G. 1984, *Phys. Rev. D*, **29**, 2683.

Peterson, J. B., Richards, P. L., and Timusk, T. 1985, *Phys. Rev. Lett.*, **55**, 332.

Roll, P. G., and Wilkinson, D. T. 1966, *Phys. Rev. Lett.*, **16**, 405.

Sironi, G., and Bonelli, G. 1987, *Ap. J.*, in press.

Smoot, G.F., *et al* 1983, *Phys. Rev. Lett.*, **51**, 1009.

——. 1985*a*, *Ap. J. Lett.*,

Smoot, G. F., De Amici, G., Levin, S., and Witebsky, C. 1985*b*, *Società Italiana di Fisica* Proceedings **1**, 27.

Smoot, G. F., Bensadoun, M., Bersanelli, M., De Amici, G., Kogut, A., Levin, S., and Witebsky, C. 1987*a*, *Ap. J. Lett.*, **317**, L345.

Smoot, G. F., De Amici, G., Levin, S., and Witebsky, C. 1987*b*, in preparation.

Stokes, R. A., Partridge, R. B., and Wilkinson, D. T. 1967, *Phys. Rev. Lett.*, **19**, 1199.

Sunyaev, R. A., and Zel'dovich, Y. B. 1970, *Ap. Space Sci.*, **7**, 20.

Witebsky, C., Smoot., G. F., De Amici, G., and Friedman, S. D. 1986, *Ap. J.*, **310**, 145.

FIGURE CAPTIONS

Figure 1. Atmospheric and peak galactic emission for a site at 3800 m elevation. The atmospheric emission is dominated by oxygen (O_2) and includes the contribution from typical water vapor column density of 0.25 g cm^{-2}.

Figure 2. Liquid-helium-cooled target used as a reference load.

Figure 3. Schematic of the radiometer.

Figure 4. Radiometer configuration in 1982. The 1983 configuration is similar with slightly larger screens.

Figure 5. Radiometer configuration in 1986.

Figure 6a. Measured 10 GHz vs 90 GHz atmospheric antenna temperature. Solid line is best fit to data excluding the 1982 results.

Figure 6b. 10 GHz zenith sky vs 90 GHz atmospheric antenna temperature. Solid line is best fit to all data.

Figure 7. Zenith sky vs calculated atmospheric antenna temperature. Solid line is the expected fit for $T_{A,\mathrm{CMBR}} = 2.38$ K.

M. Bersanelli, G. De Amici, A. Kogut, S. Levin, G. Smoot, and C. Witebsky: 50/232 Lawrence Berkeley Laboratory, University of California, Berkeley, CA 94720

S. D. Friedman: CASS C-011, University of California at San Diego, La Jolla, CA 92093

M. Griffith and B. Grossan: 37/624D Center for Space Research, Massachusetts Institute of Technology, Cambridge, MA 02139

TABLE 1

UPPER LIMITS TO SYSTEMATIC OFFSET CHANGES [a]

Year Tested	Warm Target (mK)	Cold Target (mK)
1982	15 ± 4	40 ± 8
1983	41 ± 8	43 ± 8
1984	65 ± 15	0 ± 600[b]
1986	24 ± 6	6 ± 17

[a] Warm targets are sensitive to gain and offset changes. Cold targets are sensitive only to offset changes.
[b] No precise cold measurements were made in 1984.

TABLE 2

MEASURED GAIN SATURATION

Year	Saturation (%)
1982	6 ± 1
1983	1.5 ± 1.0
1984	1.8 ± 0.2
1986	1.8 ± 0.1

TABLE 3

MEASURED ATMOSPHERIC ANTENNA TEMPERATURE [a]

Date	Time (UT)	Gain (mK/du)	T30 (K)	T40 (K)	T47 (K)	T54 (K)	$T_{A,atm}$ (K)
			1982 Primary Atmosphere[b]				
5 July	5:08–5:48	9.71 ± 0.10	1.00 ± 0.16	...	...	...	1.00 ± 0.16
	12:00–12:30	9.65 ± 0.10	0.91 ± 0.16	...	...	...	0.91 ± 0.16
6 July	3:09–3:54	9.75 ± 0.10	0.99 ± 0.16	...	...	...	0.99 ± 0.16
	6:25–7:22	9.69 ± 0.10	0.90 ± 0.16	...	...	...	0.90 ± 0.16
	11:45–12:22	9.68 ± 0.10	0.91 ± 0.16	...	...	...	0.91 ± 0.16
			1983 Primary Atmosphere				
4 Sept	8:26–9:18	8.95 ± 0.10	1.02 ± 0.28	1.21 ± 0.14	...	...	1.17 ± 0.13
5 Sept	3:32–4:17	8.95 ± 0.10	1.05 ± 0.28	1.20 ± 0.14	...	...	1.17 ± 0.13
	9:01–9:38	8.91 ± 0.10	1.06 ± 0.28	1.19 ± 0.14	...	...	1.16 ± 0.13
6 Sept	7:03–8:17	8.87 ± 0.10	1.37 ± 0.28	1.22 ± 0.14	...	...	1.25 ± 0.13
			1984 Primary Atmosphere				
24 Aug	10:36–11:27	8.86 ± 0.03	1.03 ± 0.43	1.09 ± 0.22	...	...	1.07 ± 0.20
	12:32–13:17	8.85 ± 0.03	1.00 ± 0.43	1.10 ± 0.23	...	...	1.08 ± 0.20
25 Aug	7:04–7:51	8.67 ± 0.03	1.18 ± 0.43	1.16 ± 0.22	...	...	1.17 ± 0.20
			1986 Secondary Atmosphere[c]				
8 Aug	2:53–3:34	9.24 ± 0.03	1.21 ± 0.09	1.22 ± 0.05	1.26 ± 0.03	1.27 ± 0.02	1.25 ± 0.07
	10:12–11:38	9.13 ± 0.03	1.12 ± 0.09	1.16 ± 0.05	1.18 ± 0.03	1.22 ± 0.02	1.17 ± 0.07
9 Aug	3:11–4:18	9.49 ± 0.03	1.29 ± 0.09	1.27 ± 0.05	1.30 ± 0.03	1.32 ± 0.02	1.30 ± 0.07
	9:14–10:06	9.17 ± 0.03	1.12 ± 0.09	1.17 ± 0.05	1.20 ± 0.03	1.22 ± 0.02	1.18 ± 0.07

[a] Quantities T30, T40, T47, and T54 (columns 4–7) are the mean atmospheric antenna temperatures for ±30°, ±40°, ±47°, and ±54°, respectively. $T_{A,atm}$ is the appropriately weighted mean value (see text). A du is a digiitized unit of radiometer output. Errors quoted are 68% confidence level limits.

[b] The uncertainty for $T_{A,atm}$ for 1982 may be an underestimate (see text).

[c] Prior to 1986, only primary atmospheric measurements were made. For 1986, only the more accurate secondary results are shown.

TABLE 4

COMPARISON OF 1986 PRIMARY AND SECONDARY ATMOSPHERIC MEASUREMENTS[a]

Date (1986)	Time (UT)	Linear Drift (mK/hour)	Primary $T_{A,\mathrm{atm}}$ (K)	Secondary $T_{A,\mathrm{atm}}$ (K)
8 Aug	4:40–5:27	-11 ± 1	1.24 ± 0.12	1.23 ± 0.07
	7:48–8:24	...	1.19 ± 0.12	1.20 ± 0.07
9 Aug	5:51–6:21	-23 ± 7	1.17 ± 0.12	1.24 ± 0.07
	7:35–8:11	...	1.15 ± 0.12	1.20 ± 0.07

[a] The quoted errors are 68% confidence level limits and include systematic uncertainties.

TABLE 5

CALCULATED ATMOSPHERIC ANTENNA TEMPERATURE [a]

Date (1982)	Time (UT)	Measured 90 GHz $T_{A,\mathrm{atm}}$ (K)[b]	Measured 10 GHz $T_{A,\mathrm{atm}}$ (K)	Calculated 10 GHz $T_{A,\mathrm{atm}}$ (K)
5 July	5:08–5:48	13.58 ± 0.57	1.00 ± 0.16	1.19 ± 0.11
	12:00–12:30	...	0.91 ± 0.16	...
6 July	3:09–3:54	14.08 ± 0.57	0.99 ± 0.16	1.20 ± 0.11
	9:01–9:38	13.34 ± 0.57	0.90 ± 0.16	1.19 ± 0.11
	11:45–12:22	...	0.91 ± 0.16	...

[a] Quoted uncertainties are 68% confidence level limits. The "Measured 10 GHz" uncertainty (column 4) may be an underestimate (see text).
[b] Simultaneous 90 GHz values are not available for some observing times.

TABLE 6

CONTRIBUTIONS TO ATMOSPHERIC SYSTEMATIC ERROR [a]

Source Term	Approximate Source Magnitude	Approximate Source Uncertainty	Atmospheric Error (mK) 30°	40°
Offset Changes	0 mK	43 mK	269	135
Pointing Repeatability	0′	4′	10	6
Gain	9 mK/du	0.10 mK/du	12	12
Sidelobes	5 mK	3 mK	19	10
Galaxy	25 mK	12 mK	39	19
Atm Model	...	3%	38	36
Total			275	142
Weighted Total			126	

[a] The values shown are for 1983. Similar values hold for 1984, with larger offset uncertainty. The 1986 error has no offset term but has an additional observed 63 mK effect.

TABLE 7

CONTRIBUTIONS TO CMBR SYSTEMATIC ERROR

Source Term	Approximate Value	CMBR Error (mK) 1982	1983	1984	1986
Atmosphere	1.15 K	110	130	200	65
Offset Change	0 mK	40	43	65	17
Gain	9 mK/du	<1	<1	<1	<1
Cold Load	3.562 K	13	13	13	13
Ground	0 mK	3	3	3	3
Galaxy	4 mK	3	2	2	4
Total		118	138	211	69

TABLE 8

TERMS USED TO CALCULATE CMBR ANTENNA TEMPERATURE [a]

Date		Time (UT)	Number Of Scans	$G\Delta V$ (mK)	$T_{A,\mathrm{load}}$ (mK)	$T_{A,\mathrm{atm}}$ (mK)	$T_{A,\mathrm{ground}}$ (mK)	$T_{A,\mathrm{galaxy}}$ (mK)
1982	5 July	5:08–5:48	15	48 ± 41	3562 ± 13	1189 ± 110	0 ± 3	3 ± 3
	6 July	3:09–3:54	18	72 ± 41		1195 ± 110		3 ± 3
		6:25–7:22	22	65 ± 40		1185 ± 110		3 ± 3
1983	4 Sept	8:26–9:18	15	−24 ± 43	3562 ± 13	1170 ± 130	0 ± 3	3 ± 3
	5 Sept	3:32–4:17	13	46 ± 44		1165 ± 130		5 ± 3
		9:01–:38	9	32 ± 44		1162 ± 130		3 ± 3
	6 Sept	7:03–8:17	23	106 ± 45		1253 ± 130		4 ± 3
1984	24 Aug	10:36–11:27	13	−53 ± 65	3562 ± 13	1074 ± 195	0 ± 3	4 ± 2
		12:32–13:17	9	−94 ± 67		1075 ± 205		3 ± 2
	25 Aug	7:04–7:51	12	34 ± 65		1166 ± 195		8 ± 4
1986	8 Aug	7:48–8:24	9	8 ± 37	3568 ± 13	1197 ± 65	0 ± 3	5 ± 3
	9 Aug	5:51–6:21	8	40 ± 35		1240 ± 65		15 ± 8
		7:35–8:11	9	−68 ± 33		1201 ± 65		7 ± 4

[a] The quoted errors are 68% confidence level limits and include systematic uncertainties. $G\Delta V$ (column 4) refers to the measured zenith sky − cold load temperature difference.

TABLE 9

CMBR RESULTS FOR 1982–1986 [a]

Year	Number of Observations	$T_{A,CMBR}$ (K)	Statistical RMS (K)	CMBR Thermodynamic Temperature (K)
1982	55	2.430	0.035	2.66 ± 0.12
1983	61	2.401	0.069	2.63 ± 0.14
1984	34	2.419	0.045	2.65 ± 0.21
1986	26	2.331	0.093[b]	2.56 ± 0.08
Combined:				2.61 ± 0.06

[a] The errors of the CMBR thermodynamic temperature are 68% confidence level limits and include systematic effects. The combined result is a weighted average of the results of the four years.

[b] The 1986 data are not well-described by a Gaussian distribution (see text).

TABLE 10

RECENT MEASUREMENTS OF CMBR THERMODYNAMIC TEMPERATURE

References	Wavelength (cm)	Frequency (GHz)	T_{CBR} (K)
Sironi *et al.* 1987	50.0	0.6	2.45 ± 0.70
Levin (Smoot *et al.* 1987*a*)	21.2	1.41	2.22 ± 0.55
Sironi (Smoot *et al.* 1985*b*)	12.0	2.5	2.78 ± 0.13
De Amici (De Amici *et al.* 1987)	8.1	3.7	2.58 ± 0.13
Mandolesi *et al.* 1986	6.3	4.75	2.70 ± 0.07
Kogut *et al.* 1987[a]	3.0	10.0	2.61 ± 0.06
Johnson and Wilkinson 1986	1.2	24.8	2.783 ± 0.025
De Amici (Smoot *et al.* 1985*b*)	0.909	33.0	2.81 ± 0.12
Bersanelli and Witebsky (Smoot *et al.* 1987*a*)	0.333	90.0	2.60 ± 0.10
Meyer & Jura 1985	0.264	113.6	2.70 ± 0.04
Meyer & Jura 1985	0.132	227.3	2.76 ± 0.20
Crane *et al.* 1986	0.264	113.6	2.74 ± 0.05
Crane *et al.* 1986	0.132	227.3	$2.75^{+0.24}_{-0.29}$
Peterson,	0.351	85.5	2.80 ± 0.16
Richards, &	0.198	151	$2.95^{+0.11}_{-0.12}$
Timusk 1985	0.148	203	2.92 ± 0.10
	0.114	264	$2.65^{+0.09}_{-0.10}$
	0.100	299	$2.55^{+0.14}_{-0.18}$

[a] This work

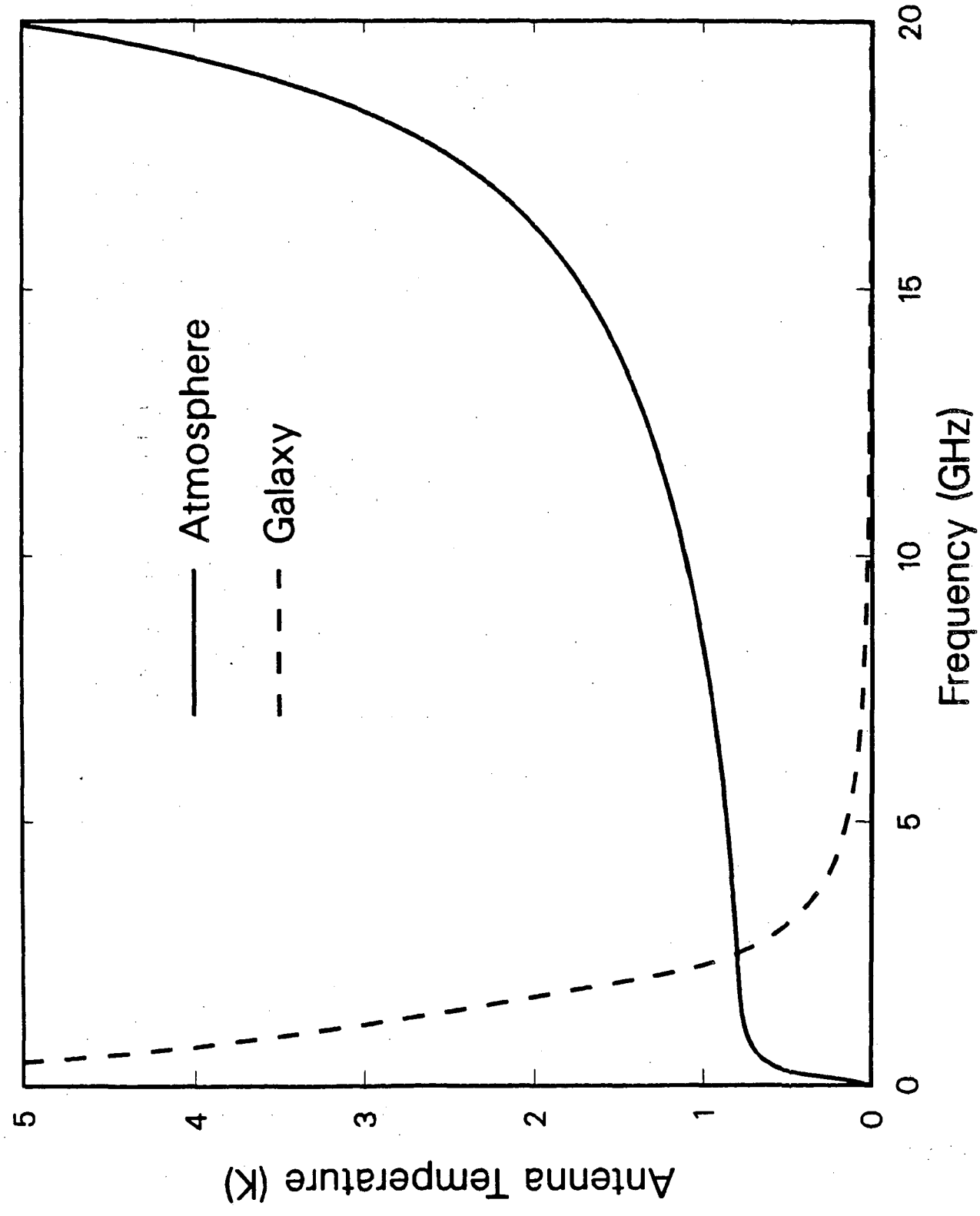
Antenna Temperature (K)
0
1
2
3
4
5
Frequency (GHz)
0
5
10
15
20
Atmosphere
Galaxy

Fig. 1

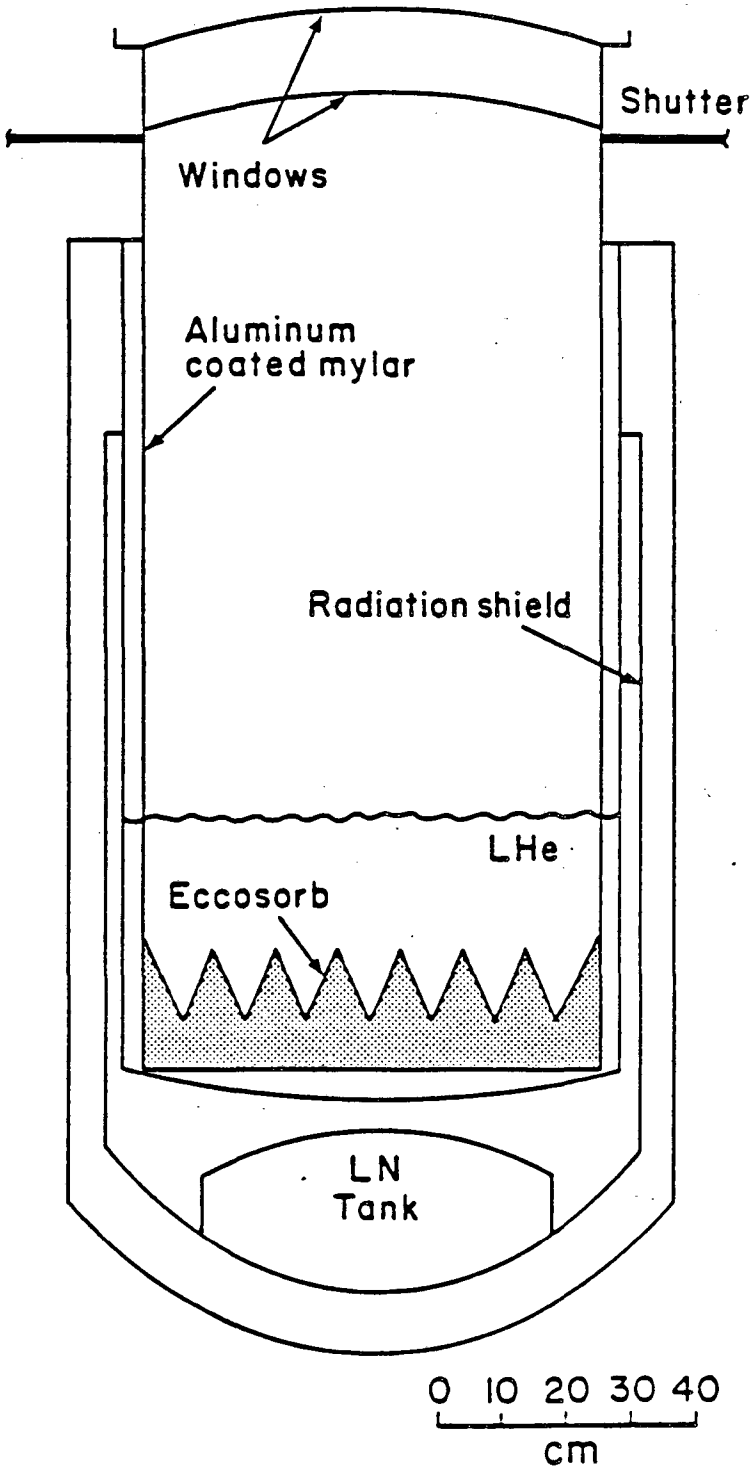
Shutter
Windows
Aluminum
coated mylar
Radiation shield
LHe
Eccosorb
LN
Tank
0 10 20 30 40
cm

Fig. 2

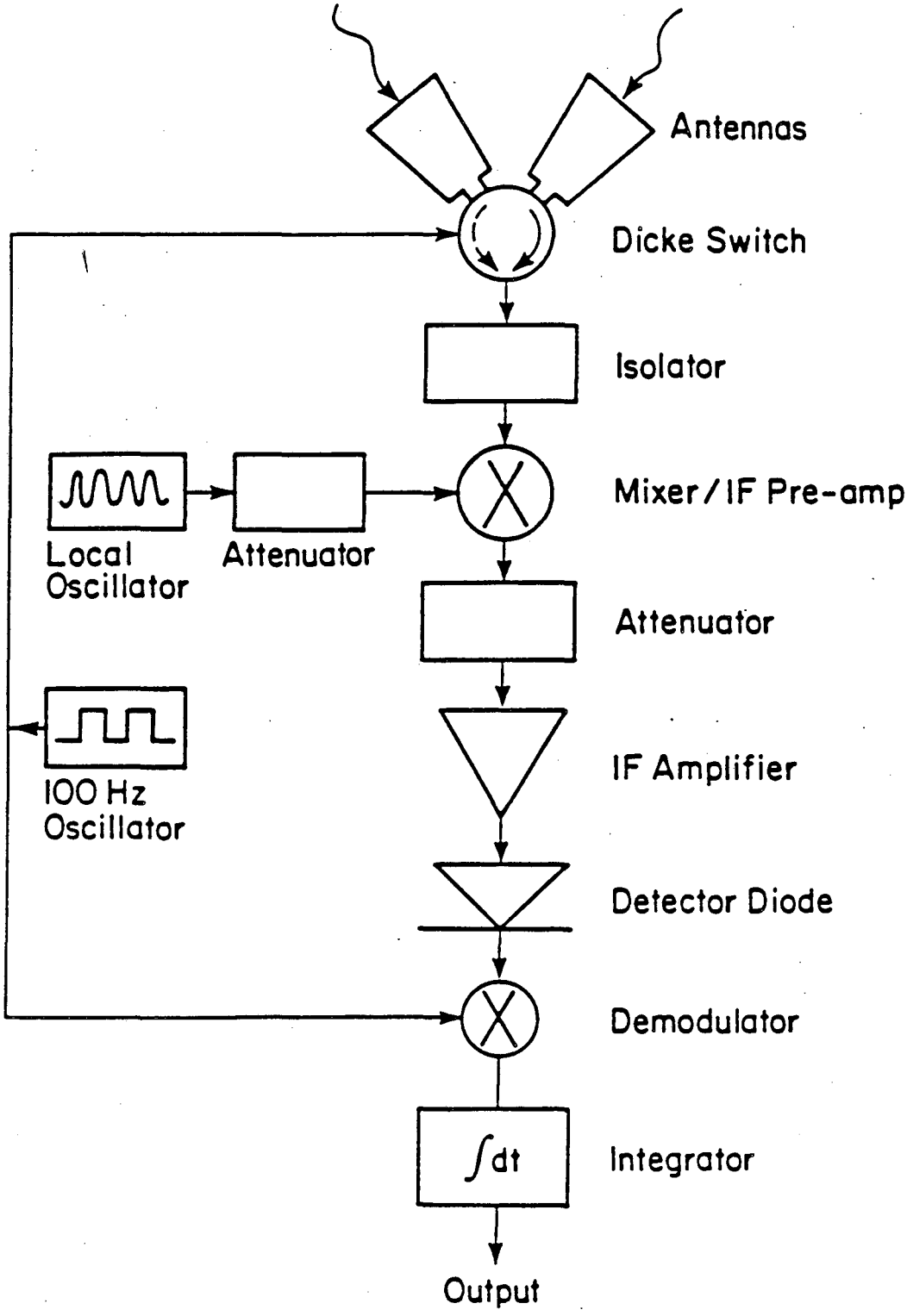
Antennas
Dicke Switch
Isolator
Mixer / IF Pre-amp
Local Oscillator
Attenuator
Attenuator
IF Amplifier
100 Hz Oscillator
Detector Diode
Demodulator
∫dt
Integrator
Output

Fig. 3

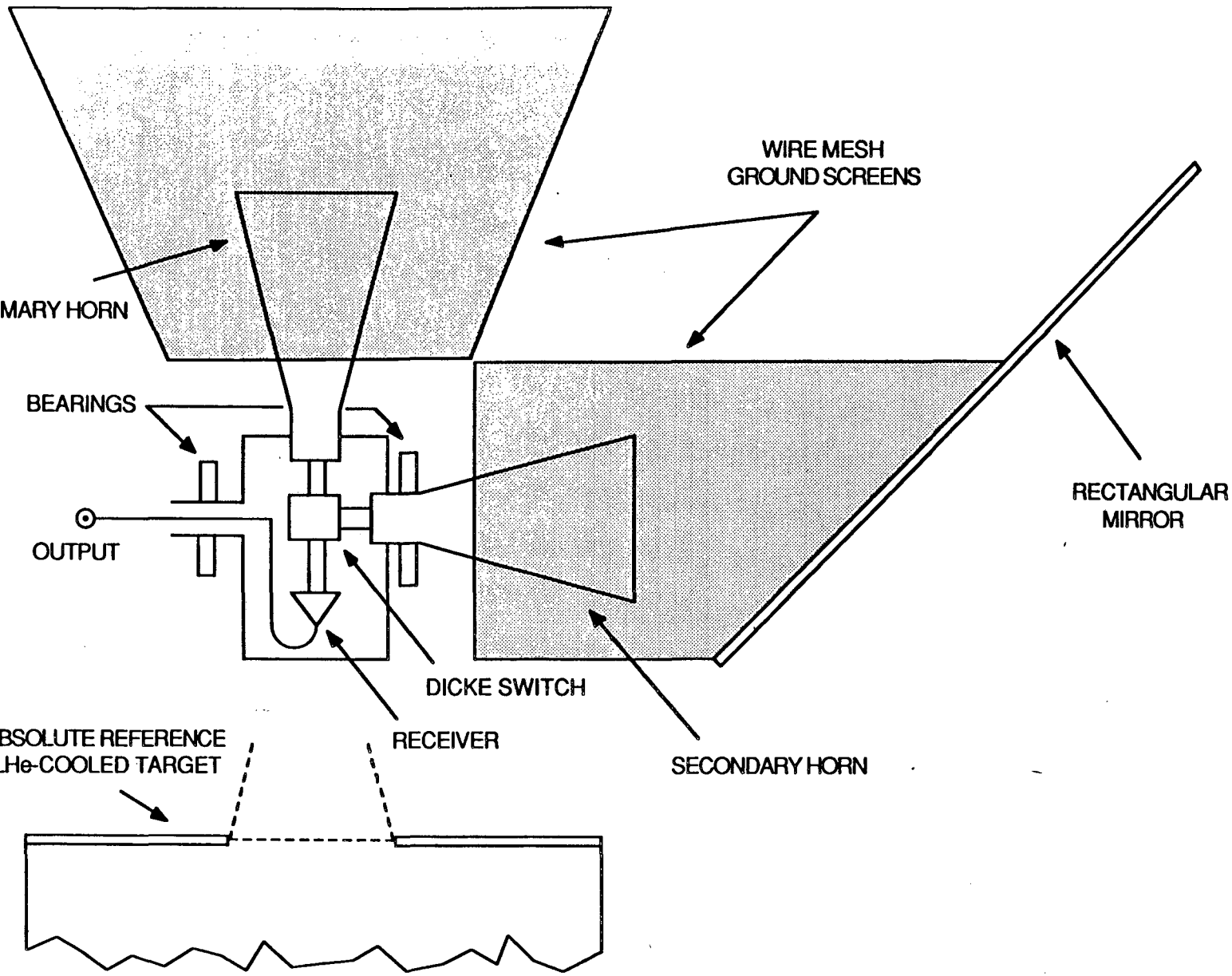
WIRE MESH
GROUND SCREENS
PRIMARY HORN
BEARINGS
OUTPUT
RECTANGULAR
MIRROR
DICKE SWITCH
RECEIVER
SECONDARY HORN
ABSOLUTE REFERENCE
LHe-COOLED TARGET

Fig. 4

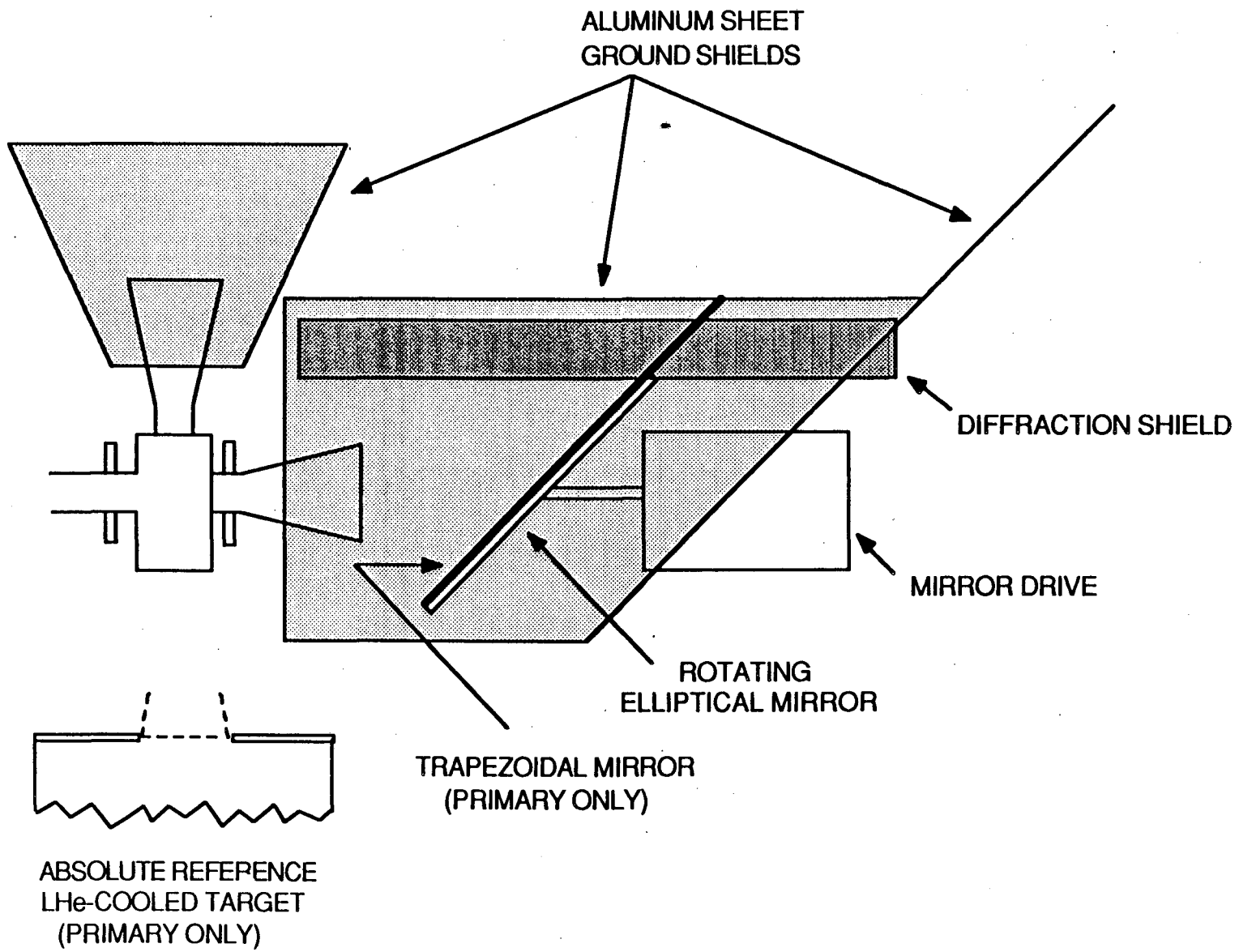
ALUMINUM SHEET
GROUND SHIELDS
DIFFRACTION SHIELD
MIRROR DRIVE
ROTATING
ELLIPTICAL MIRROR
TRAPEZOIDAL MIRROR
(PRIMARY ONLY)
ABSOLUTE REFERENCE
LHe-COOLED TARGET
(PRIMARY ONLY)

Fig. 5

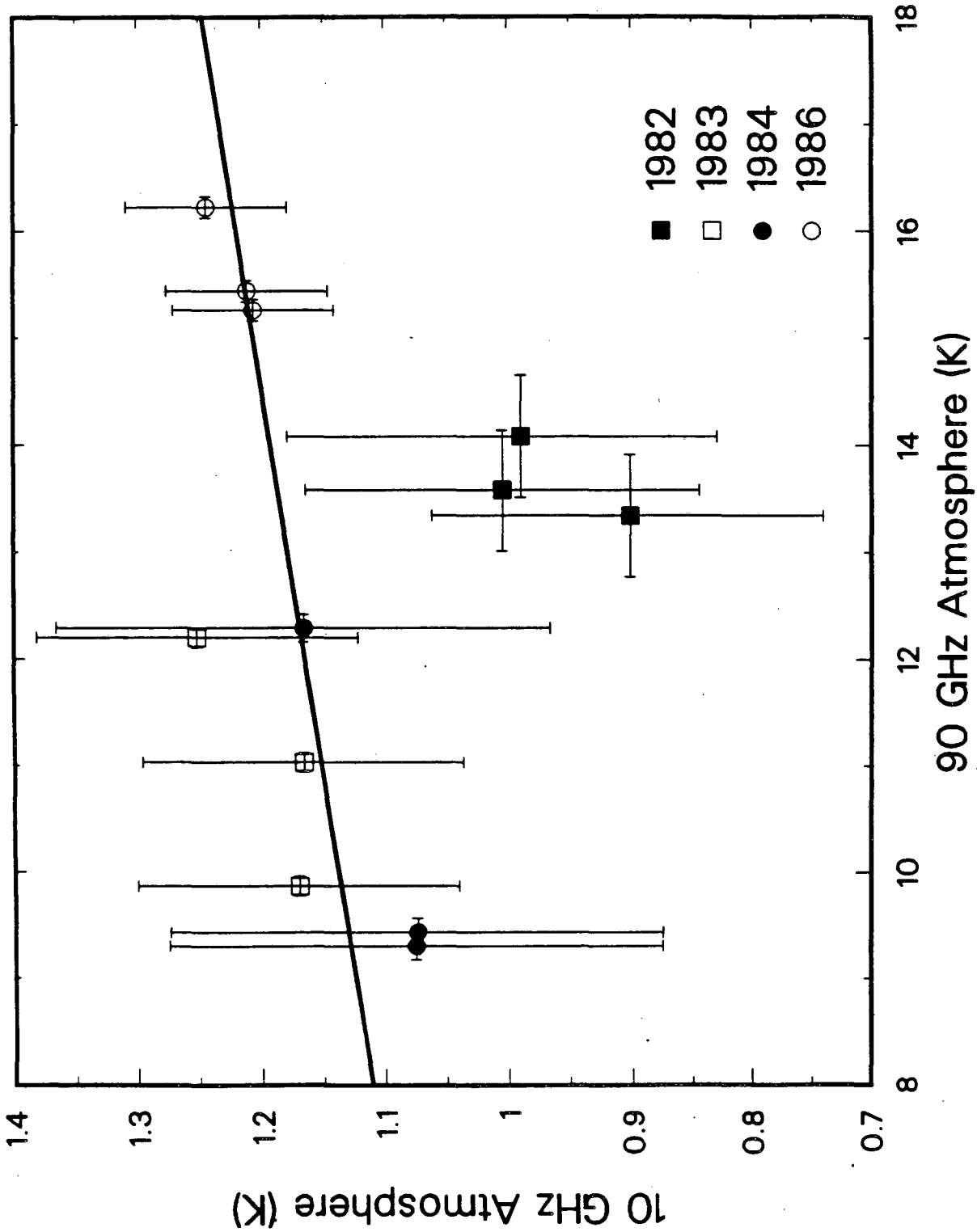
1982
1983
1984
1986
90 GHz Atmosphere (K)
10 GHz Atmosphere (K)
8
10
12
14
16
18
0.7
0.8
0.9
1
1.1
1.2
1.3
1.4

Fig. 6a

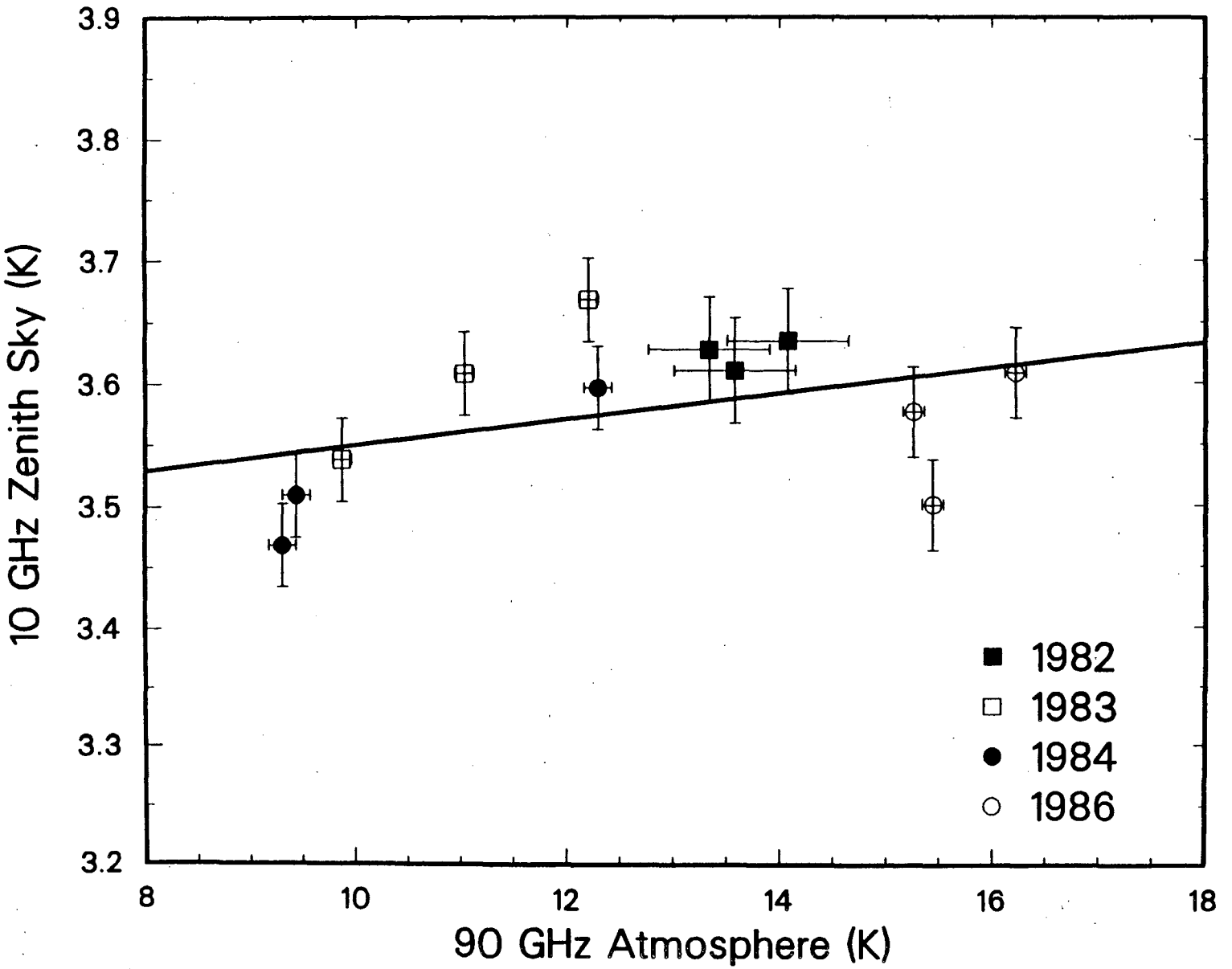
3.9
3.8
3.7
3.6
3.5
3.4
3.3
3.2
10 GHz Zenith Sky (K)
8
10
12
14
16
18
90 GHz Atmosphere (K)
1982
1983
1984
1986

Fig. 6b

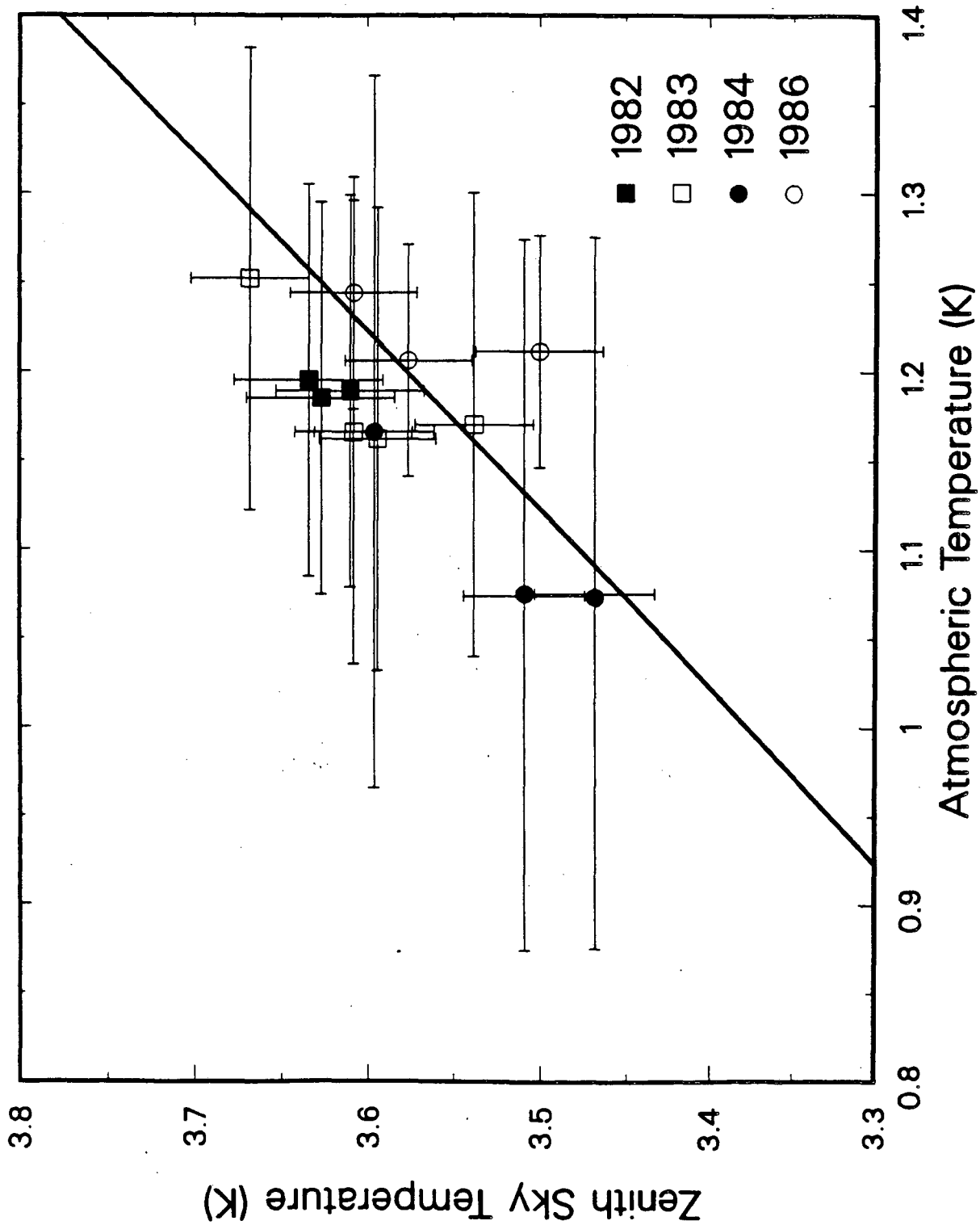
Zenith Sky Temperature (K)
3.8
3.7
3.6
3.5
3.4
3.3
Atmospheric Temperature (K)
0.8
0.9
1
1.1
1.2
1.3
1.4
1982
1983
1984
1986

Fig. 7

LAWRENCE BERKELEY LABORATORY
TECHNICAL INFORMATION DEPARTMENT
UNIVERSITY OF CALIFORNIA
BERKELEY, CALIFORNIA 94720